Journal of Solid State Chemistry 182 (2009) 3003–3012

Contents lists available at ScienceDirect

Journal of Solid State Chemistry

journal homepage: www.elsevier.com/locate/jssc

Crystal structure, spectroscopy and thermodynamic properties of $M^{I}VWO_6$(M^{I} – Li, Na)

Aleksandr V. Knyazev [a,*], Miroslaw Mączka [b], Nataliya N. Smirnova [a], Lucyna Macalik [b], Nataliya Yu. Kuznetsova [a], Irene A. Letyanina [a]

[a] Nizhny Novgorod State University, Gagarin Prospekt 23/2, 603950 Nizhny Novgorod, Russia
[b] Institute of Low Temperature and Structure Research, Polish Academy of Sciences, P.O. Box 1410, 50-950 Wroclaw, Poland

ARTICLE INFO

Article history:
Received 29 April 2009
Received in revised form
6 August 2009
Accepted 7 August 2009
Available online 14 August 2009

Keywords:
Brannerite
Heat capacity
Thermodynamic functions
IR and Raman spectroscopy
Absorbance
X-ray diffraction

ABSTRACT

In the present work lithium (sodium) vanadium tungsten oxides with brannerite structure is refined by the Rietveld method (space group $C2/m$, $Z=2$). IR and Raman spectroscopy was used to assign vibrational bands and determine structural particularities. The diffuse reflectance spectra allow to calculate bandgap for $M^{I}VWO_6$(M^{I} – Li, Na). The temperature dependences of heat capacity have been measured first in the range from 7 to 350 K for these compounds and then between 330 and 640 K, respectively, by precision adiabatic vacuum and dynamic calorimetry. The experimental data were used to calculate standard thermodynamic functions, namely the heat capacity $C_p^o(T)$, enthalpy $H^o(T)-H^o(0)$, entropy $S^o(T)-S^o(0)$ and Gibbs function $G^o(T)-H^o(0)$, for the range from $T\rightarrow 0$ to 640 K. The differential scanning calorimetry was applied to measure decomposition temperature of compounds under study.

1. Introduction

Compounds with brannerite structure [15] containing alkali metal atoms can be used as materials for independent supply source. There is information about $LiVMoO_6$ and $LiVWO_6$ and their use in lithium-ion batteries [1]. Besides materials on basis of $M^{I}VWO_6$ compounds can be used as catalysts due to content of transition metals.

The object of our investigation is complex oxides containing vanadium, tungsten and alkali metals. In order to understand the relations among structure and energetics in a fundamental sense, and to correlate reactivity at high temperature and materials compatibility in applications, thermodynamic data are essential. Despite the extensive interest in vanadium tungsten oxides, there is no any thermodynamic data and other physicochemical data are presented in bare number of publications. Therefore, detailed investigations of these compounds are especially important.

The goals of this work include detailed structural and spectroscopic investigations, studies of thermal stability, calorimetric determination of the temperature dependence of the heat capacity $C_p^o = f(T)$ of $LiVWO_6$ and $NaVWO_6$ from 7 to 640 K, detection of the possible phase transitions, and calculation of the standard thermodynamic functions $C_p^o(T)$, $H^o(T)-H^o(0)$, $S^o(T)-S^o(0)$ and $G^o(T)-H^o(0)$ in the range from $T\rightarrow 0$ to 640 K.

2. Experimental

2.1. Sample

Lithium (sodium) vanadium tungsten oxide samples were prepared by the solid-state reaction between tungsten oxide, vanadium oxide and alkali metal nitrate, respectively [1]. The synthesis was performed in a porcelain crucible, into which the reaction mixture with the atomic ratio1Li (Na):1W:1V was loaded. The mixture was calcined at 873 K for 20 h, undergoing regrinding every 5 h. For structural investigations, X-ray diffraction patterns of $LiVWO_6$ and $NaVWO_6$ samples were recorded on a Shimadzu X-ray diffractometer XRD-6000 (Cu$K\alpha$ radiation, geometry θ–2θ) in the 2θ range from 10° to 120° with scan increment of 0.02°. Rietveld analysis and structure refinement [2] were carried out using RIETAN-94 software [3]. The X-ray data and estimated impurity content (0.5–1 wt%) in the substances led us to conclude that the studied sample were individual crystalline compounds.

2.2. Apparatus and measurement procedure

To measure the heat capacity C_p^o of the tested substances in the range from 7 to 350 K a BKT-3.0 automatic precision adiabatic

* Corresponding author. Fax: +7 831 434 50 56.
E-mail address: knav@uic.nnov.ru (A.V. Knyazev).

0022-4596/$ - see front matter © 2009 Elsevier Inc. All rights reserved.
doi:10.1016/j.jssc.2009.08.010

vacuum calorimeter with discrete heating was used. The calorimeter design and the operation procedure were described earlier [4,5]. The calorimeter was tested by measuring the heat capacity of high-purity copper and reference samples of synthetic corundum and K-2 benzoic acid. The analysis of the results showed that measurement error of the heat capacity of the substance at helium temperature was within ±2%, then it decreased to ±0.5% as the temperature was rising to 40 K, and was equal to ±0.2% at $T>40$ K. Temperatures of phase transitions can be determined with the error of ±0.02 K.

To measure the heat capacity of the sample between 330 and 650 K an automatic thermoanalytical complex (ADKTTM) – a dynamic calorimeter operating by the principle of triple thermal bridge was used [6,7]. The device design and the measurement procedure of the heat capacity, temperatures and enthalpies of phase transitions were demonstrated in detail in the above-mentioned papers. The reliability of the calorimeter operation was checked by measuring the heat capacity of the standard sample of synthetic corundum as well as the thermodynamic characteristics of fusion of indium, tin and lead. As a result, it was found that the calorimeter and the measurement technique allow one to obtain the heat capacity values of the substances in solid and liquid states with the maximum error of ±1.5% and the phase transition temperatures within ca. ±0.5 K. Since the heat capacity of the examined compound was also measured between 330 and 350 K in the adiabatic vacuum calorimeter with the error of ±0.2% and the conditions of measurements in the dynamic device were chosen so that in the above temperature interval the C_p^o values measured with the use of both calorimeters coincided, it was assumed that at $T>395$ K the heat capacity was determined with the error of 0.5–1.5%. The data on the heat capacity of the objects under study were obtained in the range from 330 to 650 K at the average rate of heating of the calorimeter and the substances of 0.0333 K/s.

Thermal behavior was carried out with DSC Labsys from Setaram in a platinum crucible ranging from 293 to 1173 K (heating rate 0.167 K/s).

Polycrystalline infrared spectra were measured with a Biorad 575C FT-IR spectrometer in KBr suspension for the 1200–400 cm^{-1} region and in Nujol suspension for the 500–50 cm^{-1} region. FT-Raman spectra were measured using BRUKER 110/S spectrometer. Excitation was performed with a 1064 nm line of a YAG:Nd^{3+} laser. Both IR and Raman spectra were recorded with a spectral resolution of 2 cm^{-1}.

Room-temperature diffuse reflectance spectra were obtained in the 200–2500 nm spectral region using a Cary-Varian 5E UV–vis–near-IR spectrophotometer and diffuse reflectance accessory.

3. Results and discussion

3.1. Crystal structure

The structure of $LiVWO_6$ and $NaVWO_6$ was refined assuming space group $C2/m$. The initial model included the atomic coordinates in the structure of $NaVMoO_6$ [1,8]. The details of the X-ray diffraction experiment and structure refinement data are listed in Table 1. Fig. 1 represents the measured, simulated and difference X-ray diffraction patterns for $LiVWO_6$ and $NaVWO_6$, as well as a pattern of lines corresponding to reflection maxima. There is a good agreement between the measured and simulated patterns. Table 2 lists the coordinates of the atoms and their isotropic thermal parameters. The refined model yielded positive isotropic thermal parameters B for all atoms. In the case of $NaVWO_6$, we calculated thermal parameters for all atoms types, whereas for lithium counterpart we equated their values for all light atoms in order to get positive isotropic thermal parameters in defined model. This procedure is used in powder X-ray diffraction quite often. Table 3 lists the interatomic distances and valence angles in the structure and Fig. 2 represents a fragment of the Li(Na)VWO_6 structure.

Table 1
Details of the X-ray diffraction experiment and the results of the structure refinement for M^IVWO_6 (M^I – Li, Na).

	$LiVWO_6$	$NaVWO_6$
Space group	*C2/m*	
Z	2	
2θ range (deg)	10–120	
a (Å)	9.3699(2)	9.4422(1)
b (Å)	3.67063(6)	3.67734(4)
c (Å)	6.6258(2)	7.2345(1)
β (deg)	112.134(2)	111.769(1)
V (Å^3)	211.090(9)	233.284(6)
Number of reflections	191	226
Number of refined parameters	36	37
Structural parameters	14	16
Others	22	21
R_{wp}; R_p(%)	8.38; 5.23	5.13; 2.85

Definition of reliability factors R_{wp} and R_p are given as follows: $R_{wp} = \{(\Sigma w_i[y_{i\,obs}-y_{i\,calc}]^2/(\Sigma w_i[y_{i\,obs}]^2)\}^{1/2}$; $R_p = (\Sigma|y_{i\,obs}-y_{i\,calc}|)/(\Sigma y_{i\,obs})$.

As we can see from the obtained X-ray diffraction data the compounds under investigation have quasi-layered structure. The VWO_6^- layers consist of distorted V(W)-octahedra jointed by edges. The alkali metal atoms are located in the interlayer space forming M^IO_6-polyhedra. The M^IO_6-polyhedra are composed of three oxygen atoms from one layer and three similar oxygen atoms from neighboring layer. In case of $NaVWO_6$, the coordination of sodium ions is close to octahedral, although there is a slight compression of the octahedron along axial axis in this structure and its tendency towards tetragonal–pyramidal environment. In $LiVWO_6$, the LiO_6-polyhedron is tetragonal bipyramid, in which the difference between equatorial and axial bond distances is equal to 0.472 Å. The alkali metal coordination polyhedra are joined by edges forming linear (one-dimensional) chains.

Analysis of the unit cell parameters shows that the lattice parameters (a and b) of Li(Na)VWO_6 are very similar and these values slightly increase when moving from $LiVWO_6$ to $NaVWO_6$ by 0.77% and 0.18%, respectively. In contrast to this behavior, the unit cell along crystallographic direction c expands significantly (by 9.2%) when Li^+ is replaced by Na^+. This behavior is connected with smaller compression of Na-coordination polyhedron than Li-polyhedron leading to increase of the unit cell volume by 10.5%.

In order to establish the crystal-chemical borders in alkali metal vanadium tungsten oxides, we have analyzed several compounds with brannerite structure. It was determined that only negligible quantity of compounds could crystallize in this structure type. $M^IV A^{VI}O_6$ (M^I – Li, Na, K; A^{VI} – Mo, W) [1,8,17], $M^{II}V_2O_6$ (M^{II} – Mg, Ca, Zn, Cd, Mn) [9–13] and $M^{IV}Ti_2O_6$ (M^{IV} – U, Th) [15,14] compounds are among them. Consequently, there are small atoms (0.54 Å$\le r\le$0.61 Å) with +4, +5, +6 oxidation numbers in the layers and average size atoms (0.72 Å$\le r\le$1.38 Å) with +1, +2, +4 oxidation numbers in the interlayer space. These criteria allow to suppose that complex vanadium tungsten oxides with large alkali metals could not crystallize in brannerite structure. Such conclusion was confirmed in paper [16], where authors indicated $CsVWO_6$ as compound with pyrochlore structure and cubic system (space group $F\,d3m$).

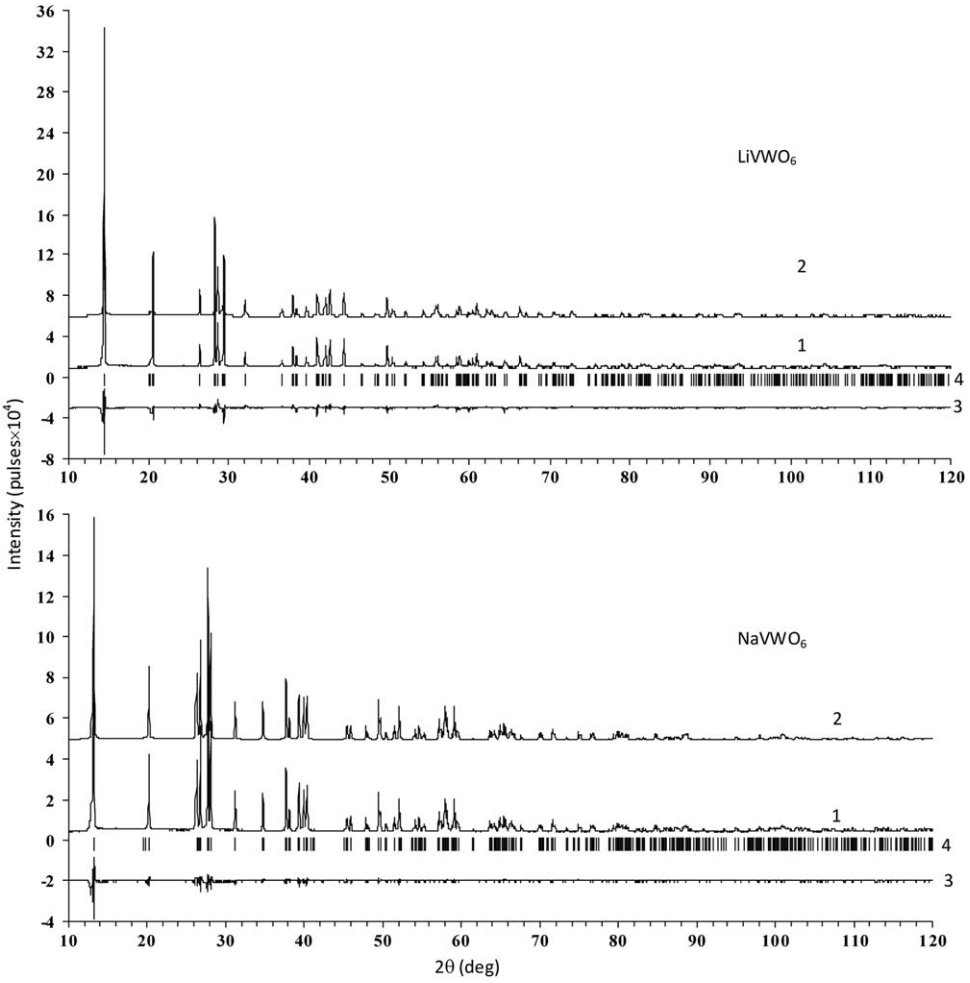

Fig. 1. Fragments of (1) observed, (2) simulated, and (3) difference X-ray diffraction patterns for $LiVWO_6$ and $NaVWO_6$, (4) Bragg reflections. The simulated pattern is shifted relative to the observed pattern.

Table 2
Coordinates and isotropic thermal parameters of atoms in the structure of $M^{I}VWO_6$ (M^{I} – Li, Na).

Atom	Site	*x*	*y*	*z*	Occ	*B* (Å²)
LiVWO₆						
Li	2a	0	0	0		0.6(1)
V	4i	0.8159(2)	0	0.3543(2)	0.5	1.40(6)
W	4i	0.8159(2)	0	0.3543(2)	0.5	1.40(6)
O(1)	4i	0.982(1)	0	0.291(1)		0.6(1)
O(2)	4i	0.690(1)	0	0.111(1)		0.6(1)
O(3)	4i	0.293(1)	0	0.413(1)		0.6(1)
NaVWO₆						
Na	2a	0	0	0		1.6(2)
V	4i	0.8180(1)	0	0.3663(2)	0.5	0.25(3)
W	4i	0.8180(1)	0	0.3663(2)	0.5	0.25(3)
O(1)	4i	0.9752(8)	0	0.310(1)		1.0(2)
O(2)	4i	0.6711(9)	0	0.135(1)		0.9(2)
O(3)	4i	0.3094(8)	0	0.438(1)		0.3(2)

3.2. Raman and IR

The structure of $LiVWO_6$ and $NaVWO_6$ is composed of MeO_6 (Me = W,V) and LiO_6 (NaO_6) polyhedra [18]. Factor group analysis predicts for this structure ($C2/m$ (C_{2h}^3) space group) $8A_g+4B_g+5A_u+10B_u$ Brillouin zone center modes. These modes can be subdivided into A_u+2B_u and $2A_g+B_g+A_u+2B_u$ translations of the Li^+ (Na^+) and Me^{6+} cations, respectively. It should be remembered, however, that among the translational modes two modes (A_u+2B_u)

Table 3
Interatomic distances and valence angles in the structure of $M^{I}VWO_6$ (M^{I} – Li, Na).

Bond	*d* (Å)	Angle	ω (deg)
LiVWO₆			
V/W–O(1)	1.760(9)	O(1)–V/W–O(1a)	78.1(7)
V/W–O(2)	1.598(9)	O(1)–V/W–O(2)	98.3(8)
V/W–O(3) (× 2)	1.903(2)	O(1)–V/W–O(3)(× 2)	102.9(8)
V/W–O(3a)	2.152(9)	O(1a)–V/W–O(3)(× 2)	84.7(7)
V/W–O(1a)	2.401(9)	O(1a)–V/W–O(3)	73.1(7)
		O(2)–V/W–O(3)(× 2)	96.2(8)
		O(2)–V/W–O(3a)	110.6(8)
		O(3a)–V/W–O(3)(× 2)	74.7(7)
Li–O(1) (× 2)	1.995(9)	O(1)–Li–O(2)(× 4)	91.4(8)
		O(1a)–Li–O(2)(× 4)	88.6(8)
Li–O(2) (× 4)	2.467(8)	O(2a)–Li–O(2)(× 2)	83.9(8)
		O(2a)–Li–O(2)(× 2)	96.1(8)
NaVWO₆			
V/W–O(1)	1.677(8)	O(1)–V/W–O(1a)	76.4(4)
V/W–O(2)	1.733(9)	O(1)–V/W–O(2)	103.3(5)
V/W–O(3) (× 2)	1.921(2)	O(1)–V/W–O(3)(× 2)	101.3(5)
V/W–O(3a)	2.169(6)	O(1a)–V/W–O(3)(× 2)	80.7(4)
V/W–O(1a)	2.428(6)	O(1a)–V/W–O(3a)	79.3(4)
		O(2)–V/W–O(3)(× 2)	99.4(5)
		O(2)–V/W–O(3a)	101.0(5)
		O(3a)–V/W–O(3)(× 2)	74.5(4)
Na–O(1) (× 2)	2.343(8)	O(1)–Na–O(2)(× 4)	84.4(4)
		O(1a)–Na–O(2)(× 4)	95.6(5)
Na–O(2) (× 4)	2.403(6)	O(2a)–Na–O(2)(× 2)	80.2(4)
		O(2a)–Na–O(2)(× 2)	99.9(5)

a – atoms sites O: 1−*x*, 0, 1−*z*.

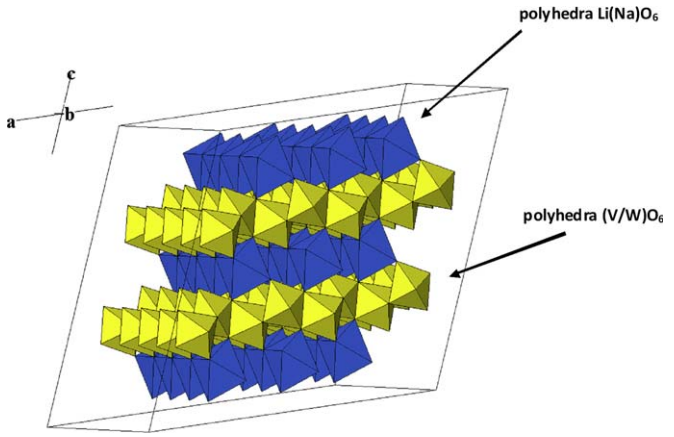

Fig. 2. Fragment of the structure of Li(Na)VWO_6.

belong to the acoustic branches. The remaining modes ($6A_g+3B_g+3A_u+6B_u$) correspond to vibrations of the oxygen atoms. The A_g and B_g modes are Raman active, and the A_u and B_u modes are IR active.

The Raman spectra show presence of very strong bands at 968 and 965 cm^{-1} for $LiVWO_6$ and $NaVWO_6$, respectively (see Fig. 3). The 968 cm^{-1} band of $LiVWO_6$ was assigned previously to vibrations of the terminal V═O groups [19]. Since tungsten and vanadium ions occupy statistically the same sites in the crystal structure, we assign this band to vibrations of the terminal Me═O groups. The corresponding IR bands are observed as clear doublets near 956–973 cm^{-1} (see Table 4 and Fig. 3). The IR spectra show also presence of weak bands near 936–934 cm^{-1} which can be most likely assigned to some overtones or combination bands.

The bands of $LiVWO_6$ in the regions 809–886 and 576–754 cm^{-1} were assigned previously to asymmetric stretching vibrations of the V–O–V bonds running parallel to the *b*-axis and V_2O_2 groups, respectively [19]. Closer inspection of the structure shows, however, that all MeO_6 octahedra running parallel to the *b*-axis share edges, not corners. As a result no single oxygen bridges of the type V–O–V are present in the structure but the Me ions are joined along the *b*-axis through double oxygen bridges MeOOMe with the shorter (Me–O) and longer (Me⋯O) distances equal to 1.905 and 2.175 Å or 1.903 and 2.152 Å according to Ref. [18] and our present X-ray data, respectively. This double oxygen bridge will be denoted as type I. These adjacent chains of the MeO_6 octahedra running parallel to the *b*-axis also share edges forming double oxygen bridges with the Me–O and Me⋯O distances of 1.687 and 2.379 or 1.760 and 2.401 Å according to Ref. [18] and our present X-ray data, respectively. This bridge will be denoted as type II. We assign the 809–886 and 576–754 cm^{-1} bands of $LiVWO_6$ to stretching vibrations of asymmetric bridge II and symmetric bridge I, respectively. The corresponding bands for bridge I of $NaVWO_6$ are observed at very similar wavenumbers but the bands assigned by us to bridge II are significantly shifted towards higher wavenumbers (up to 12 cm^{-1}). Inspection of the structure shows that the oxygen atoms which take part in formation of bridge I are well separated from the Li^+ (Na^+) ions whereas the oxygen atoms taking part in formation of bridge II have close contacts with Li^+ ions. As a result the substitution of Li^+ by Na^+ should have significant influence only on bridge II. Indeed, our X-ray results show that whereas the Me–O and Me⋯O distances for bridge I are very similar for both $LiVWO_6$ and $NaVWO_6$ (see Table 3), the Me–O bond in bridge II is much shorter for $NaVWO_6$ (1.677 Å) than $LiVWO_6$ (1.760 Å). The observed shift of bands in the 809–886 cm^{-1} region towards higher wavenumbers

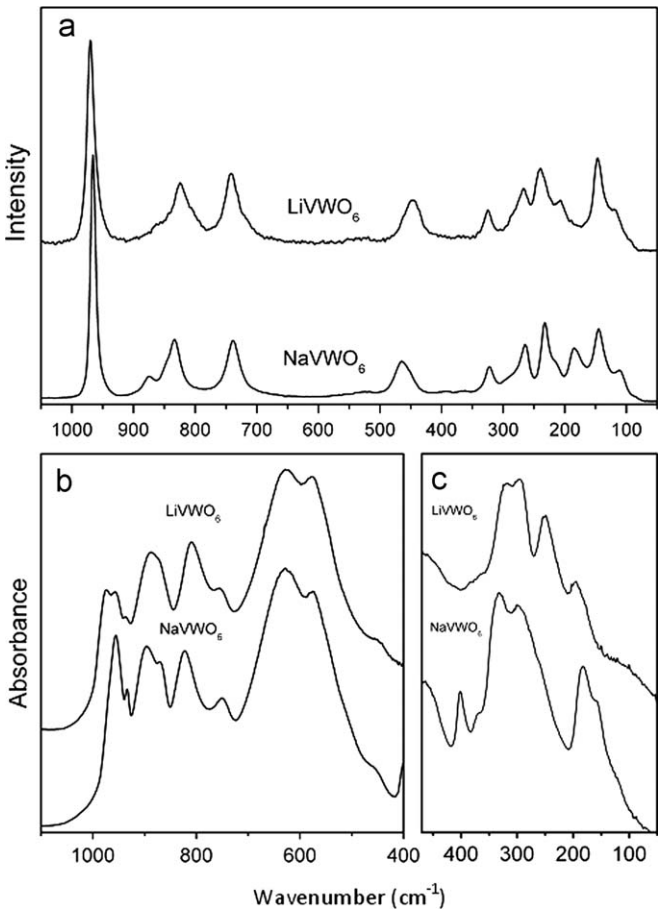

Fig. 3. Raman (a), mid-IR (b) and far-IR (c) spectra of $LiVWO_6$ and $NaVWO_6$.

Table 4
Raman and IR wavenumbers for $LiVWO_6$ and $NaVWO_6$ together with the proposed assignment.

$LiVWO_6$		$NaVWO_6$		Assignment
Raman	IR	Raman	IR	
968s	973m	965s	968sh	ν(Me = O)
–	956m	–	956m	
–	936w	–	934w	Overtone or combination band
861sh	886s	874w	896m	ν(MeOMeO) type II
–	–	847sh	870w	
823m	809s	832m	823m	
740m	754w	737m	749w	ν(MeOMeO) type I
719sh	–	–		
–	625s	–	628s	
–	576s	–	573m	
–	–	519vw	–	Overtone or combination band
446m	448sh	463m	453w	δ(MeOMeO) type II
–	383vw	–	401w	δ(MeOMeO) type I and II
–	363w	–	368w	
324w	318s	322w	332s	
279sh	295s	282sh	297s	
266m	–	264m	–	
–	251m	–	182m	δ(MeOMeO)+T′(Li^+) (or T′(Na^+)
238m	–	231m	–	δ(MeOMeO) type I
206w	–	216sh	–	
–	195w	–	159w	T′(Me^{6+})+T′(Li^+) (or T′(Na^+)
–	–	183m		T′(Me^{6+})
146m		144m		
118w		110w		

for $NaVWO_6$ supports, therefore, our assignment of these bands to vibrations of bridge II and it is consistent with significant shortening of the Me–O bond. Amdouni et al. [19] also suggested that the weak Raman band near 519 cm^{-1} can be assigned to symmetric stretching of the Me–O–Me bridges. It is very well known that symmetric vibrations give usually rise to strong Raman bands and weak IR bands whereas asymmetric vibrations are usually observed as strong IR and weak Raman bands. Very weak intensity of the Raman band at 519 cm^{-1} and its relatively large bandwidth suggest that this band should be assigned to an overtone or a combination band, rather than to the symmetric stretching mode.

Amdouni et al. [19] also assigned the band of $LiVWO_6$ at 446 cm^{-1} to symmetric stretching of the Me–O–Me bridges. Numerous studies of crystals containing WO_6 or VO_6 octahedra showed that stretching modes are usually observed above 500 cm^{-1} but in some cases can also be observed in the 400–500 cm^{-1} range [20–22]. We propose to assign the band at 446 cm^{-1} to bending mode of the double oxygen bridge II because this band is well separated from the stretching modes and similarly as in the case of bridge II stretching modes, this band is significantly shifted towards higher wavenumbers for $NaVWO_6$. The IR and Raman bands in the 295–401 and 206–324 cm^{-1} range, respectively, can be assigned to bending modes of the both oxygen bridges. Amdouni et al. also suggested that translations of Li^+ ions contribute significantly to the IR bands at 252 and 295 cm^{-1}. Replacement of Li^+ (atomic mass 6.94) by much heavier Na^+ ions (atomic mass 22.99) should lead to wavenumber decrease of the pure translational mode by a factor of $(22.99/6.94)^{0.5} = 1.82$. Our results show, however, the 295 cm^{-1} band of $LiVWO_6$ shifts to 297 cm^{-1} for $NaVWO_6$. Therefore, the contribution of the alkali metal translational motions to this band is negligible. In contrast to this behavior, the IR band at 251 cm^{-1} for $LiVWO_6$ shifts to 182 cm^{-1} for $NaVWO_6$ indicating that it has significant contribution of alkali metal translation. The bands below 200 cm^{-1} were assigned previously to the lattice modes [19]. We confirm this conclusion and assign the Raman bands at 183, 144–146 and 110–118 cm^{-1} to three expected translations of the Me^{6+} ions.

3.3. Absorption

The diffuse reflectance spectra of the $LiVWO_6$ and $NaVWO_6$ samples are shown in Fig. 4. The spectra exhibit strong increase of absorption at wavelengths lower than 560 and 510 nm for $LiVWO_6$ and $NaVWO_6$, respectively, due to the bandgap transition. For indirect bandgap material, the absorption coefficient satisfies the equation $(\alpha h\nu)^{1/2} = A(h\nu - E_g)$, where α, ν, A and E_g are absorption coefficient, light frequency, proportionality coefficient and bandgap energy, respectively [23]. The bandgap obtained by extrapolation of the plots (insets in Fig. 4) of $(\alpha h\nu)^{1/2}$ versus $h\nu$ are 1.73 eV for $LiVWO_6$ and 2.24 eV for $NaVWO_6$, respectively. These results indicate that the both materials have a bandgap suitable for photocatalitic applications in the visible range. The observed shift of the optical bandgap from 1.73 eV for $LiVWO_6$ to 2.24 eV for $NaVWO_6$ is consistent with the change of the sample color from light brown to nearly yellow. The bandgap values are significantly lower than those obtained for WO_3 (2.6–3.5 eV) [24,25]. However, the former studies of $(WO_3)_{1-x}(V_2O_5)_x$ system indicated that the bandgap decreases with increasing concentration of V_2O_5 [24]. It is also worth noting that for $LiVWO_6$ a broad band is observed at about 1570 nm. The origin of this band is not clear.

3.4. Heat capacity

The C_p^o measurements were carried out between 7 and 640 K. The masses of the sample loaded in the calorimetric ampoules of the BKT-3.0 and ADKTTM devices were, respectively, 0.8662 and 1.7536 g for $LiVWO_6$ and 1.8008 and 2.0893 g for $NaVWO_6$. In the BKT-3.0 calorimeter, 154 (for $LiVWO_6$) 187 (for $NaVWO_6$) experimental C_p^o values were obtained in two series of experiments. The heat capacity of the sample varied from 30% to 70% of the total heat capacity of calorimetric ampoule + substance over the range between 7 and 640 K. The experimental points of C_p^o in the temperature interval between $T = (7$ and $640)$ K were fitted by means of the least-squares method and polynomial equations (Eqs. (1)–(3)) of the C_p^o versus temperature have been obtained. The corresponding coefficients (A, B, C, etc.) are given in Tables 5 and 6

$$C_p^o(T) = A + B\cdot(T/30) + C\cdot(T/30)^2 + D\cdot(T/30)^3 + E\cdot(T/30)^4 + F\cdot(T/30)^5 + G\cdot(T/30)^6 + H\cdot(T/30)^7 + I\cdot(T/30)^8 + J\cdot(T/30)^9 \quad (1)$$

$$C_p^o(T) = A + B\cdot ln(T/30) + C\cdot\{\ln(T/30)\}^2 + D\cdot\{\ln(T/30)\}^3 + E\cdot\{\ln(T/30)\}^4 + F\cdot\{\ln(T/30)\}^5 + G\cdot\{\ln(T/30)\}^6 + H\cdot\{\ln(T/30)\}^7 + I\cdot\{\ln(T/30)\}^8 + J\cdot\{\ln(T/30)\}^9 \quad (2)$$

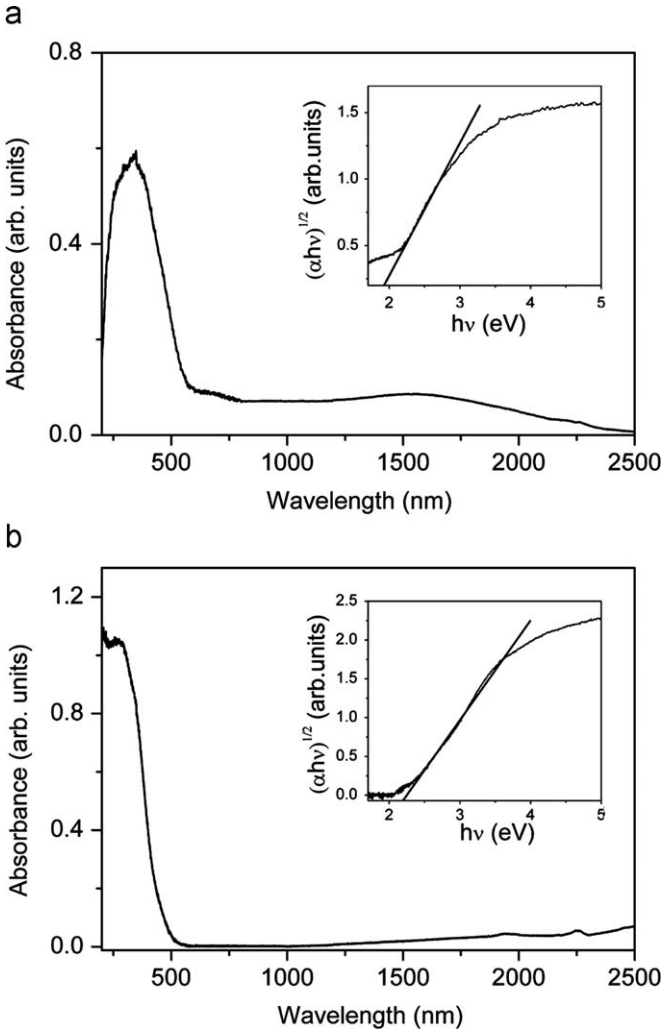

Fig. 4. Diffuse reflectance spectra of $LiVWO_6$ (a) and $NaVWO_6$ (b).

Table 5
Coefficients in the fitting polynomials for $LiVWO_6$.

T (K)	7–30	25–90	80–150	140–300	290–350	320–640
polynomial's type	3	2	1	1	1	3
Coefficients/(J K^{-1} mol^{-1})						
A	-3.6241651×10^{0}	2.6610007×10^{-2}	-7.7001978×10^{1}	-3.4389084×10^{1}	2.9331286×10^{2}	-2.0568188×10^{2}
B	2.1901629×10^{0}	6.0037994×10^{-2}	1.4835328×10^{2}	3.4184999×10^{1}	-1.2128672×10^{2}	3.5034258×10^{2}
C	1.2225779×10^{0}	9.0867199×10^{-2}	-1.2128155×10^{2}	-1.4321943×10^{1}	1.4743014×10^{1}	-2.3635515×10^{2}
D	1.4938465×10^{1}	-7.0653025×10^{-3}	5.4572672×10^{1}	3.2986871×10^{0}	6.2081003×10^{-1}	7.8277315×10^{1}
E	5.5310068×10^{1}	-5.0250122×10^{-1}	-1.4586421×10^{1}	-4.5040924×10^{-1}	-3.2181278×10^{-1}	-1.2638648×10^{1}
F	1.0220721×10^{2}	1.7167388×10^{0}	2.3157741×10^{0}	3.6460391×10^{-2}	3.2291259×10^{-2}	7.8877237×10^{-1}
G	9.6758300×10^{1}	-2.4457200×10^{0}	-2.0222951×10^{-1}	-1.6206739×10^{-3}	-1.4313383×10^{-3}	–
H	4.4957192×10^{1}	1.6720786×10^{0}	7.4952069×10^{-3}	3.0526544×10^{-5}	2.4527543×10^{-5}	–
I	8.1451825×10^{0}	-4.4894228×10^{-1}	–	–	–	–

Table 6
Coefficients in the fitting polynomials for $NaVWO_6$.

T (K)	7–30	25–90	80–210	200–350	330–670
polynomial's type	2	2	1	1	2
Coefficients/(J K^{-1} mol^{-1})					
A	1.0833723×10^{1}	1.0800909×10^{1}	-2.6715897×10^{3}	-5.9335143×10^{2}	8.1365915×10^{4}
B	2.3832551×10^{1}	2.3157301×10^{1}	4.8197386×10^{3}	3.4784517×10^{2}	-9.9376981×10^{4}
C	3.9811517×10^{1}	4.5023005×10^{1}	-3.7268310×10^{3}	-6.8759964×10^{1}	2.0912572×10^{3}
D	1.5654327×10^{2}	3.8973428×10^{0}	1.6322010×10^{3}	7.0110843×10^{0}	4.8545706×10^{4}
E	5.3300325×10^{2}	-7.0096752×10^{2}	-4.4015000×10^{2}	-3.5694960×10^{-1}	-2.4904509×10^{4}
F	1.0657268×10^{3}	3.1255171×10^{3}	7.4827423×10^{1}	7.2006490×10^{-3}	1.9127266×10^{3}
G	1.2480316×10^{3}	-6.368789×10^{3}	-7.8358675×10^{0}	–	1.7932505×10^{3}
H	8.4603910×10^{2}	6.8968280×10^{3}	4.6240030×10^{-1}	–	-5.3448355×10^{2}
I	3.0744427×10^{2}	-3.8397244×10^{3}	-1.1779155×10^{-2}	–	4.5957745×10^{1}
J	4.6342847×10^{1}	8.6460434×10^{2}	–	–	–

$$\ln C_p^{o}(T) = A + B\cdot\ln(T/30) + C\cdot\{\ln(T/30)\}^2 + D\cdot\{\ln(T/30)\}^3 + E\cdot\{\ln(T/30)\}^4 + F\cdot\{\ln(T/30)\}^5 + G\cdot\{\ln(T/30)\}^6 + H\cdot\{\ln(T/30)\}^7 + I\cdot\{\ln(T/30)\}^8 + J\cdot\{\ln(T/30)\}^9 \quad (3)$$

Their root mean square deviation from the averaging $C_p^{o} = f(T)$ curve was $\pm0.15\%$ in the range $T = (6–30)$ K, $\pm0.075\%$ from $T = (25–150)$ K, $\pm0.15\%$ between $T = (130$ and $350)$ K and $\pm0.5\%$ over the range from $T = (370–650)$ K.

The experimental values of the molar heat capacity of Li(Na)VWO_6 over the range from 7 to 640 K and the averaging $C_p^{o} = f(T)$ plot are presented in Fig. 5 and Tables 9 and 10. The heat capacity C_p^{o} of this substance gradually increases with rising temperature and does not show any peculiarities until 640 K.

3.5. Standard thermodynamic functions

To calculate the standard thermodynamic functions (Tables 7 and 8) of the lithium (sodium) vanadium tungsten oxides, their C_p^{o} values were extrapolated from the starting temperature of the measurement (approximately 7 K) to 0 K by Debye's function of heat capacity:

$$C_p^{o} = nD(\theta_D/T) \quad (4)$$

where D is the symbol of Debye's function, $n = 6$ and $\theta_D(LiVWO_6) = 215.4$ K as well as $\theta_D(NaVWO_6) = 200.4$ K are specially selected parameters. Eq. (4) with the above parameters describes the experimental C_p^{o} values of the compound between 7 and 12 K with the error of $\pm1.69\%$ and $\pm1.77\%$, respectively.

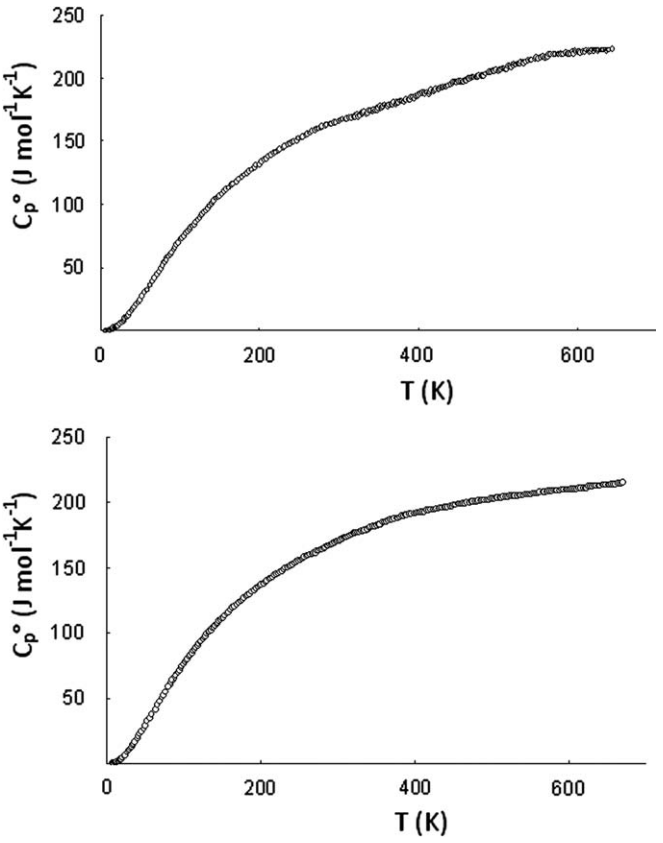

Fig. 5. Temperature dependences of heat capacity of $LiVWO_6$ and $NaVWO_6$.

Table 7
Thermodynamic functions of crystalline $LiVWO_6$; $M(LiVWO_6) = 337.7289\ g\ mol^{-1}$, $p^\circ = 0.1$ MPa.

T (K)	$C_p^\circ(T)$ ($J\ K^{-1}\ mol^{-1}$)	$H^\circ(T)-H^\circ(0)$ ($kJ\ mol^{-1}$)	$S^\circ(T)$ ($J\ K^{-1}\ mol^{-1}$)	$-[G^\circ(T)-H^\circ(0)]$ ($kJ\ mol^{-1}$)
0	0	0	0	0
5	0.0486	0.0001	0.0162	0.00002
10	0.3785	0.0010	0.1295	0.000318
15	1.517	0.0052	0.4584	0.001658
20	3.475	0.0175	1.150	0.005514
25	6.010	0.0409	2.185	0.01373
30	8.990	0.0783	3.540	0.02791
35	12.78	0.1323	5.199	0.04963
40	16.93	0.2066	7.177	0.08043
45	21.05	0.3015	9.408	0.1218
50	25.39	0.4175	11.85	0.1749
60	34.29	0.7161	17.27	0.3199
70	43.64	1.105	23.24	0.5220
80	53.11	1.589	29.69	0.7864
90	62.74	2.170	36.52	1.117
100	71.57	2.841	43.59	1.518
110	79.46	3.598	50.79	1.989
120	86.35	4.427	58.00	2.533
130	93.50	5.326	65.19	3.149
140	100.9	6.298	72.40	3.837
150	107.3	7.340	79.58	4.597
160	112.9	8.441	86.69	5.429
170	118.0	9.597	93.69	6.331
180	123.0	10.80	100.6	7.302
190	128.0	12.06	107.4	8.342
200	132.9	13.36	114.1	9.449
210	137.4	14.71	120.6	10.62
220	141.6	16.11	127.1	11.86
230	145.4	17.54	133.5	13.16
240	148.9	19.02	139.8	14.53
250	152.4	20.52	145.9	15.96
260	155.8	22.06	152.0	17.45
270	159.2	23.64	157.9	19.00
273.15	160.1	24.14	159.8	19.50
280	162.0	25.25	163.8	20.61
290	164.1	26.88	169.5	22.27
298.15	165.9	28.22	174.1	23.67
300	166.3	28.53	175.1	24.00
310	168.3	30.20	180.6	25.78
320	170.2	31.89	185.9	27.61
330	172.2	33.61	191.2	29.49
340	174.4	35.34	196.4	31.43
350	176.6	37.09	201.5	33.42
360	178.6	38.87	206.5	35.46
370	180.6	40.67	211.4	37.55
380	182.6	42.48	216.2	39.69
390	184.6	44.32	221.0	41.88
400	186.6	46.18	225.7	44.11
410	188.7	48.05	230.3	46.39
420	190.7	49.95	234.9	48.72
430	192.8	51.87	239.4	51.09
440	194.9	53.81	243.9	53.50
450	197.0	55.77	248.3	55.96
460	199.1	57.75	252.6	58.47
470	201.2	59.75	256.9	61.02
480	203.2	61.77	261.2	63.61
490	205.2	63.81	265.4	66.24
500	207.2	65.87	269.6	68.92
510	209.1	67.95	273.7	71.63
520	210.9	70.05	277.8	74.39
530	212.7	72.17	281.8	77.19
540	214.3	74.31	285.8	80.03
550	215.8	76.46	289.8	82.90
560	217.2	78.62	293.7	85.82
570	218.5	80.80	297.5	88.78
580	219.6	82.99	301.3	91.77
590	220.5	85.19	305.1	94.80
600	221.3	87.40	308.8	97.87
610	221.9	89.62	312.5	101.0
620	222.4	91.84	316.1	104.1
630	222.6	94.07	319.6	107.3
640	222.7	96.29	323.1	110.5

Table 8
Thermodynamic functions of crystalline $NaVWO_6$; $M(NaVWO_6) = 353.77767\ g\ mol^{-1}$, $p^\circ = 0.1$ MPa.

T (K)	$C_p^\circ(T)$ ($J\ K^{-1}\ mol^{-1}$)	$H^\circ(T)-H^\circ(0)$ ($kJ\ mol^{-1}$)	$S^\circ(T)$ ($J\ K^{-1}\ mol^{-1}$)	$-[G^\circ(T)-H^\circ(0)]$ ($kJ\ mol^{-1}$)
0	0	0	0	0
5	0.0604	0.0001	0.0201	0.000025
10	0.4696	0.0012	0.1610	0.000395
15	1.868	0.0065	0.5672	0.002057
20	4.244	0.0215	1.415	0.006813
25	7.283	0.0500	2.674	0.01689
30	10.81	0.0951	4.309	0.03419
35	15.24	0.1598	6.296	0.06056
40	20.03	0.2480	8.644	0.09776
45	24.69	0.3598	11.27	0.1475
50	29.55	0.4953	14.12	0.2109
60	39.24	0.8398	20.38	0.3828
70	49.10	1.281	27.15	0.6201
80	58.73	1.821	34.35	0.9274
90	68.17	2.457	41.83	1.308
100	76.43	3.180	49.44	1.764
110	84.59	3.985	57.11	2.297
120	92.18	4.870	64.80	2.907
130	99.09	5.827	72.46	3.593
140	105.6	6.850	80.04	4.356
150	111.8	7.938	87.54	5.194
160	117.6	9.085	94.94	6.106
170	122.8	10.29	102.2	7.092
180	127.7	11.54	109.4	8.150
190	132.5	12.84	116.4	9.280
200	137.0	14.19	123.3	10.48
210	141.0	15.58	130.1	11.75
220	145.0	17.01	136.8	13.08
230	148.9	18.48	143.3	14.48
240	152.4	19.99	149.7	15.95
250	155.8	21.53	156.0	17.47
260	158.9	23.10	162.2	19.07
270	162.0	24.71	168.2	20.72
273,15	162.9	25.22	170.1	21.25
280	164.9	26.34	174.2	22.43
290	167.9	28.00	180.0	24.20
298,15	170.2	29.38	184.7	25.69
300	170.8	29.70	185.8	26.03
310	173.5	31.42	191.4	27.92
320	176.1	33.17	197.0	29.86
330	178.4	34.94	202.4	31.86
340	180.6	36.73	207.8	33.91
350	183.0	38.55	213.0	36.01
360	185.1	40.39	218.2	38.17
370	187.0	42.25	223.3	40.37
380	188.8	44.13	228.3	42.63
390	190.4	46.03	233.3	44.94
400	191.9	47.94	238.1	47.30
410	193.3	49.87	242.9	49.70
420	194.6	51.81	247.5	52.15
430	195.8	53.76	252.1	54.65
440	197.0	55.72	256.6	57.20
450	198.1	57.70	261.1	59.78
460	199.1	59.68	265.4	62.42
470	200.1	61.68	269.7	65.09
480	201.1	63.69	274.0	67.81
490	202.0	65.70	278.1	70.57
500	202.9	67.73	282.2	73.37
510	203.8	69.76	286.2	76.22
520	204.7	71.80	290.2	79.10
530	205.5	73.85	294.1	82.02
540	206.3	75.91	297.9	84.98
550	207.0	77.98	301.7	87.98
560	207.7	80.05	305.5	91.01
570	208.4	82.13	309.2	94.09
580	209.1	84.22	312.8	97.20
590	209.7	86.31	316.4	100.3
600	210.4	88.42	319.9	103.5
610	211.0	90.52	323.4	106.7
620	211.7	92.64	326.8	110.0
630	212.3	94.76	330.2	113.3
640	213.0	96.88	333.6	116.6

Table 9
Experimental values of isobaric heat capacities of $LiVWO_6$, J/(K mol) ($M(LiVWO_6) = 337.7289\ g\ mol^{-1}$).

T (K)	C_p^o	T (K)	C_p^o	T (K)	C_p^o
Series 1		32.34	10.66	89.52	62.34
6.63	0.1162	33.52	11.59	91.71	64.17
7.07	0.1397	34.68	12.55	93.90	66.23
7.65	0.1753	36.69	14.15	96.08	68.26
8.24	0.2176	38.74	15.89	98.26	70.01
8.68	0.2527	40.75	17.58	100.44	71.94
9.32	0.3104	42.49	18.94	102.61	73.73
10.04	0.3849	44.56	20.72	104.78	75.48
10.69	0.4614	46.92	22.63	106.96	77.27
11.27	0.5559	49.40	24.85	109.12	78.97
11.81	0.6455	52.45	27.62	111.29	80.24
12.64	0.8350	55.45	30.27	113.44	81.83
13.69	1.124	58.27	32.76	115.59	83.42
14.71	1.422	62.34	36.37	117.75	84.72
15.78	1.753	65.56	39.35	119.90	86.15
16.69	2.124	68.45	42.14	122.05	87.81
17.62	2.494	71.01	44.60	124.19	89.33
18.26	2.743	73.36	46.95	126.33	90.89
18.65	2.896	75.73	49.13	128.46	92.44
19.09	3.091	80.00	53.12	130.60	93.96
19.74	3.351	84.66	57.77	132.73	95.51
20.45	3.649	88.93	61.64	134.86	97.06
22.15	4.495	Series 2		136.98	98.68
24.01	5.453	78.57	52.04	139.10	100.2
26.33	6.786	80.50	54.14	141.21	101.7
28.47	8.023	82.94	56.43	143.33	103.1
30.00	9.017	85.14	58.43	145.43	104.5
31.23	9.802	87.33	60.45	147.40	105.7
149.61	107.0	243.83	150.3	328.78	172.0
152.24	108.5	246.72	151.1	331.38	172.5
155.39	110.6	249.59	152.3	333.95	173.0
158.55	112.2	252.30	153.1	336.55	173.5
161.69	113.7	255.30	154.1	339.04	174.0
164.83	115.3	258.14	155.2	341.34	174.4
167.50	116.6	260.96	156.1	343.81	174.9
170.50	118.1	263.76	157.1	346.36	175.4
174.19	120.2	266.55	158.2	348.83	176.0
177.68	122.0	269.32	159.1	351.27	176.5
181.16	123.7	272.08	159.7	Series 3[a]	
184.16	125.2	275.00	160.7	320.46	169.4
187.25	126.7	277.50	161.4	326.33	170.7
190.32	128.2	279.40	161.8	332.20	173.8
193.39	129.4	282.21	162.4	338.08	174.8
196.41	131.2	285.00	163.1	343.95	176.0
199.37	132.6	288.10	163.7	349.83	176.6
202.41	134.0	290.55	164.2	355.70	177.5
205.44	135.6	294.11	165.1	361.57	177.6
208.47	136.7	296.87	165.6	367.45	179.5
211.48	138.0	299.40	166.1	372.40	180.8
214.49	139.3	302.10	166.7	379.20	181.9
217.49	140.6	304.82	167.3	385.07	184.4
220.48	141.6	307.54	167.8	390.94	185.5
223.46	142.8	310.70	168.5	396.82	186.0
226.43	144.1	312.93	168.9	402.69	188.0
229.38	145.4	315.60	169.4	408.57	188.1
232.32	146.4	318.27	169.9	414.44	189.1
235.24	147.3	320.91	170.4	420.25	190.8
238.16	148.3	323.55	170.9	425.94	191.2
241.08	149.3	326.00	171.4	431.53	193.9
437.02	193.5	511.40	207.7	587.88	219.9
444.26	196.1	516.81	208.7	593.34	220.2
449.66	196.2	522.32	210.7	598.78	220.3
455.06	197.6	527.79	211.8	604.21	220.6
460.49	198.9	533.34	212.1	611.37	222.0
465.89	201.3	538.81	213.7	616.77	222.1
471.35	201.4	546.15	214.6	622.21	222.2
476.78	203.3	551.69	216.1	627.72	222.5
482.21	203.4	557.18	217.1	633.18	222.6
489.52	205.0	562.60	217.2	638.64	222.7
494.98	205.6	569.76	218.1		
500.42	205.7	576.98	218.2		
505.85	207.3	582.41	218.8		

[a] Each third value of C_p^o .

Table 10
Experimental values of isobaric heat capacities of $NaVWO_6$, J/(K mol) ($M(NaVWO_6) = 353.77767\ g\ mol^{-1}$).

T (K)	C_p^o	T (K)	C_p^o	T (K)	C_p^o
Series 1		31.26	11.86	87.04	65.65
6.83	0.06215	32.41	12.84	88.86	67.20
7.15	0.2332	33.69	14.00	90.67	68.70
7.77	0.2425	34.73	14.97	92.48	70.20
8.32	0.2729	36.82	16.97	94.20	71.70
8.69	0.3127	38.76	18.85	96.10	73.20
9.27	0.3801	40.89	20.87	97.90	74.75
10.14	0.4890	42.73	22.59	99.70	76.20
10.71	0.5784	44.62	24.35	101.50	77.70
11.23	0.6774	47.01	26.61	103.29	79.20
11.79	0.8030	49.52	29.06	105.09	80.60
12.55	1.004	52.63	32.14	106.88	82.10
13.63	1.346	55.68	35.14	108.67	83.57
14.70	1.746	58.39	37.73	110.44	85.00
15.64	2.137	62.43	41.55	112.23	86.26
16.65	2.586	65.78	44.81	114.01	87.70
17.57	3.014	68.67	47.74	115.78	89.02
18.14	3.288	71.17	50.29	117.56	90.30
18.61	3.519	73.45	52.56	119.33	91.62
19.00	3.714	75.84	54.86	121.10	92.92
19.69	4.071	80.03	58.77	122.86	94.17
20.30	4.399	84.72	63.41	124.62	95.45
22.08	5.424	89.03	67.41	126.38	96.61
23.97	6.607	Series 2		128.14	97.88
26.28	8.138	81.61	60.40	129.89	99.17
28.42	9.641	83.41	62.20	131.64	100.2
30.02	10.85	85.23	64.00	133.39	101.4
135.14	102.6	208.04	140.3	281.25	165.3
136.88	103.7	210.47	141.4	283.36	165.8
138.59	104.7	212.82	142.1	285.21	166.4
140.33	105.8	215.24	143.0	287.26	166.9
142.06	106.8	217.65	144.0	289.33	167.5
143.79	107.9	220.06	145.1	291.38	168.3
145.52	109.0	222.45	146.0	293.39	168.9
147.24	110.2	224.84	146.9	295.41	169.4
148.96	111.1	227.22	147.8	297.42	170.0
150.68	112.2	229.60	148.8	299.41	170.6
152.83	113.4	231.96	149.7	301.39	171.1
155.41	115.0	234.32	150.2	303.37	171.7
157.98	116.5	236.66	151.1	305.33	172.3
160.55	118.0	238.99	152.0	307.28	172.8
163.11	119.4	241.32	153.0	309.22	173.4
165.67	120.6	243.64	153.6	311.14	173.9
168.22	121.9	245.96	154.5	313.05	174.5
170.76	123.3	248.24	155.3	314.94	174.8
173.24	124.4	250.39	155.8	316.43	175.2
175.77	125.5	252.67	156.6	318.31	175.7
178.29	126.8	254.93	157.5	320.16	176.2
180.81	128.1	257.20	158.1	322.01	176.6
183.31	129.3	259.45	158.8	323.83	176.9
185.81	130.6	261.69	159.4	325.65	177.4
188.31	131.7	263.92	160.2	327.45	177.8
190.80	132.9	266.13	160.9	329.19	178.1
193.28	134.2	268.34	161.5	330.91	178.4
195.76	135.3	270.53	162.1	332.67	178.8
198.23	136.1	272.67	162.8	334.36	179.2
200.69	137.2	274.83	163.4	336.08	179.4
203.15	138.2	276.98	164.1	337.79	179.9
205.60	139.3	279.12	164.6	339.49	180.2
341.17	180.8	370.14	187.3	512.64	204.1
342.83	181.1	377.64	188.6	520.14	204.5
343.89	181.3	385.14	189.8	527.64	205.1
345.47	181.7	392.64	190.9	535.14	205.7
347.09	181.9	400.14	192.0	542.64	206.3
348.63	182.2	407.64	192.9	550.14	206.9
350.22	182.6	415.14	193.8	557.64	207.3
351.80	183.1	422.64	194.6	565.14	208.1
353.35	183.2	430.14	195.6	572.64	208.6
354.89	183.6	437.64	196.4	580.14	209.1
356.41	184.0	445.14	197.4	587.64	209.7
357.92	184.3	452.64	198.4	595.14	210.2
Series 3[a]		460.14	199.2	602.64	210.6
325.14	177.2	467.64	200.1	610.14	211.0
332.64	178.8	475.14	200.8	617.64	211.5

Table 10 (*continued*)

T (K)	C_p^o	T (K)	C_p^o	T (K)	C_p^o
340.14	180.6	482.64	201.6	625.14	212.1
347.64	182.2	490.14	202.2	632.64	212.6
354.40	183.7	497.64	202.8	640.14	213.0
362.80	185.8	505.14	203.5		

[a] Each third value of C_p^o.

In calculating the functions it was assumed that Eq. (4) reproduces the C_p^o values of Li(Na)VWO_6 at $T<7$ K with the same error. The calculations of $H^o(T)-H^o(0)$ and $S^o(T)-S^o(0)$ were made by the numerical integration of $C_p^o = f(T)$ and $C_p^o = f(\ln T)$ curves, respectively, and the Gibbs function $G^o(T)-H^o(0)$ was estimated from the enthalpies and entropies at the corresponding temperatures [26]. It was suggested that the error of the function values was $\pm 1\%$ at $T<40$ K, $\pm 0.5\%$ between 40 and 80 K, $\pm 0.2\%$ in the range from 80 to 390 K and $\pm 1.5\%$ between 390 and 650 K.

The absolute entropies of Li(Na)VWO_6 (Tables 7 and 8) and the corresponding simple substances W(cr), V (cr), Li (cr), Na (cr) [27] and O_2 (g) [28] were used to calculate the standard entropy of formation of the compounds under study at 298.15 K, $\Delta_f S^\circ$(298.15, $LiVWO_6$, cr) $= -532.1 \pm 0.7$ J K^{-1} mol^{-1} and $\Delta_f S^\circ$(298.15, $NaVWO_6$, cr) $= -543.6 \pm 0.7$ J K^{-1} mol^{-1}.

In order to correlate obtained thermodynamic and structural data, it is important to apply to the fractal version of Debye's theory. The values of the fractal dimension D – the most significant parameter of the fractal version of Debye's theory of heat capacity of solids [29,30] – were determined from the experimental data on the heat capacity of compounds under investigation. The values of D were estimated using the technique described in works [31,32] with the use of Eq. (5):

$$C_v = 3D(D+1)kN\gamma(D+1)\xi(D+1)(T/\theta_{max})^D \quad (5)$$

where N is the number of atoms in a formula unit, k the Boltzmann constant, $\gamma(D+1)$ the γ-function, $\xi(D+1)$ the Riemann ξ-function and θ_{max} is the characteristic temperature. According to Ref. [33], $D=1$ corresponds to the solids with chain structure, $D=2$ to those with a layered structure, and $D=3$ [34] to those with a spatial structure. For the tested compounds $D=2.4$ for $LiVWO_6$ and $D=2.5$ for $NaVWO_6$ at $T>30$ K correspond to the intermediate structure between layered and frame structure, that good coordinates with our X-ray diffraction data.

3.6. Differential scanning calorimetry

Joint application of the high temperature X-ray diffraction and thermal analysis (TG-DTA) made it possible to establish some peculiarities of processes taking place in the compounds under investigation during heating. Fig. 6 represents DTA curves of M^IVWO_6 (M^I – Li, Na), where we can see endothermic effects at 1022 K for $LiVWO_6$ and 1031 K for $NaVWO_6$. These effects are connected with incongruent melting. It is worth noting that melting temperatures of $LiVWO_6$ and Li_2WO_4 ($T_m = 1013$ K), as well as $NaVWO_6$ and Na_2WO_4 ($T_m = 1018$ K) are practically equal. The compounds containing sodium and having formulas M^IVO_3, $M^I_2WO_4$ and M^IVWO_6 possess higher melting temperatures than the lithium counterparts by about 5–10 K. This fact is associated with greater M^I-anion sublattice bond energy.

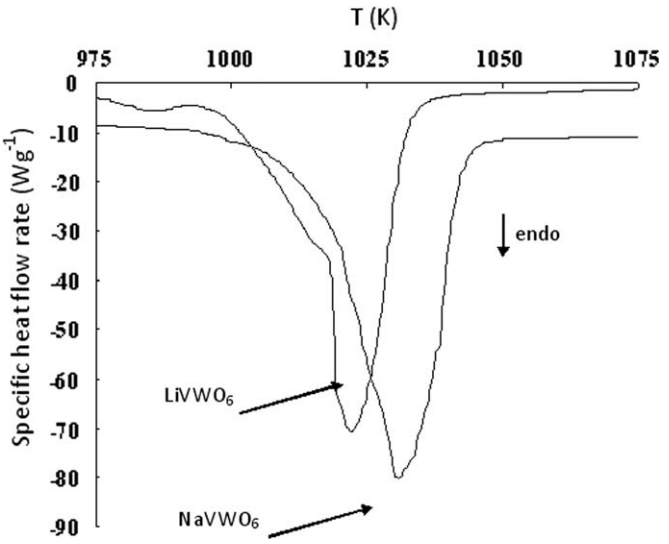

Fig. 6. Plot of the DTA-signal against temperature for $LiVWO_6$ and $NaVWO_6$.

4. Conclusions

Structure of $LiVWO_6$ and $NaVWO_6$ is refined by the Rietveld method (space group $C2/m$, $Z=2$) with R-factor 8.38% and 5.13%, respectively. Also we used IR and Raman spectroscopy for determination of structural particularities. The diffuse reflectance spectra allow to calculate bandgap for M^IVWO_6(M^I – Li, Na). These results indicate that the both materials have a bandgap suitable for photocatalytic applications in the visible range. The temperature dependences of heat capacity have been measured ranging from 7 to 640 K. The experimental data were used to calculate standard thermodynamic functions for the range from $T \to 0$ to 640 K. It was shown by the differential scanning calorimetry that these compounds are incongruent melting.

References

[1] S.R.S. Prabaharan, K. Mumtaj Begam, T.Y. Tou, M.S. Michael, Solid State Ionics 152 (2002) 91.
[2] H.M. Rietveld, Acta Crystallographica 22 (Part 1) (1967) 151.
[3] I.F. Rietveld, Analysis Programs RIETAN and PREMOS and Special Applications, In: R.A. Young (ed), The Rietveld Method, Oxford University Press, Oxford, 1993, 236pp.
[4] R.M. Varushchenko, A.I. Druzhinina, E.L. Sorkin, Journal of Chemical Thermodynamics 29 (1997) 623.
[5] V.M. Malyshev, G.A. Milner, E.L. Sorkin, V.F. Shibakin, Pribory i Tekhnika Eksperimenta 6 (1985) 195.
[6] M.Sh. Yagfarov, Zhurnal Fizicheskoi Khimii 43 (1969) 1620.
[7] A.G. Kabo, V.V. Diky, Thermochimica Acta 347 (2000) 79.
[8] B. Darriet, J. Galy, Bulletin de la Societe Francaise de Mineralogie et de Cristallographie 91 (1968) 325.
[9] H.N. Ng, C. Carlo, Canadian Journal of Chemistry 50 (1972) 3619.
[10] J.C. Bouloux, G. Perez, J. Galy, Bulletin de la Societe Francaise de Mineralogie et de Cristallographie 95 (1972) 130.
[11] G.D. Andreetti, G. Calestani, A. Montenero, Zeitschrift fuer Kristallographie 168 (1984) 53.
[12] J.C. Boloux, J. Galy, Bulletin de la Societe Chimique de France 1969 (1969) 736.
[13] H. Mueller-Buschbaum, M. Kobel, Journal of Alloys and Compounds 176 (1991) 39.
[14] J.T. Szymanski, J.D. Scott, Canadian Mineralogist 20 (1982) 271.
[15] R. Ruh, A.D. Wadsley, Acta Crystallographica 21 (1966) 974.
[16] D. Babel, G. Pausewang, W. Viebahn, Zeitschrift fuer Naturforschung 22 (1967) 1219.
[17] J. Galy, J. Darriet, D. Canals, Comptes Rendus de l Academie des Sciences 264 (1967) 1477–1480.
[18] J. Galy, G. Meunier, J. Senegas, P. Hagenmuller, Journal of Inorganic and Nuclear Chemistry 33 (1971) 2403.
[19] N. Amdouni, H. Zarrouk, C.M. Julien, Journal of Material Science 38 (2003) 4573.
[20] M. Maczka, J. Hanuza, A.F. Fuentes, U. Amador, Journal of Raman Spectroscopy 33 (2002) 56.
[21] M. Maczka, J. Hanuza, A.F. Fuentes, Y. Morioka, Journal of Physics – Condensed Matter 16 (2004) 2297.
[22] R.L. Frost, K.L. Erickson, M.L. Weir, O. Carmody, Spectrochimica Acta A 61 (2005) 829.
[23] M. Butler, Journal of Applied Physics 48 (1977) 1914.

[24] M. Ranjbar, S.M. Mahdavi, A. Iraji Zad, Solar Energy Materials and Solar Cells 92 (2008) 878.
[25] A.A. Ashkarran, A. Iraji Zad, M.M. Ahadian, S.A. Mahdavi Ardakani, Nanotechnology 19 (2008) 196709.
[26] B.V. Lebedev, Thermochimica Acta 297 (1997) 143.
[27] M.W. Chase Jr., J. Phys. Chem. Ref. Data (Monograph) 9 (1998) 1951.
[28] J.D. Cox, D.D. Wagman, V.A. Medvedev, Codata Key Values for Thermodynamics, New York, 1984.
[29] T.S. Yakubov, Doklady Akademii Nauk SSSR 310 (1990) 145.
[30] A.D. Izotov, O.V. Shebershnyova, K.S. Gavrichev, in: Third All-Union Conference on Thermal Analysis and Calorimetry, Kazan, 1996.
[31] B.V. Lebedev, A.V. Markin, V.A. Davydov, L.S. Kashevarova, A.V. Rakhmanina, Thermochimica Acta 399 (2003) 99.
[32] B.V. Lebedev, A.V. Markin, Physics of the Solid State 44 (2002) 434.
[33] V.V. Tarasov, Zhurnal Obshchei Khimii 26 (1952) 1374.
[34] V.V. Tarasov, Problems of Glass Physics, Stroyizdat, Moscow, 1979.